Surfaces, Interfaces, and Catalysis; Physical Properties of Nanomaterials and Materials

Triggering Cation Exchange Reactions by Doping

Urko Petralanda, Luca De Trizio, Graziella Gariano, Roberto Cingolani, Liberato Manna, and Sergey Artyukhin

J. Phys. Chem. Lett., **Just Accepted Manuscript** • DOI: 10.1021/acs.jpclett.8b02083 • Publication Date (Web): 07 Aug 2018

Triggering Cation Exchange Reactions by Doping

Urko Petralanda, Luca De Trizio, Graziella Gariano†, Roberto Cingolani, Liberato Manna*, Sergey Artyukhin**

Istituto Italiano di Tecnologia, Via Morego 30, Genova 16163 Italy

KEYWORDS: colloidal nanocrystals, cation exchange, DFT calculations, Wannier functions

ABSTRACT: Cation exchange (CE) reactions have emerged as a technologically important route, complementary to colloidal synthesis, to produce colloidal nanostructures of different geometries and compositions for a variety of applications. Here it is demonstrated with first-principles simulations that an interstitial impurity cation in CdSe nanocrystals weakens nearby bonds and reduces the CE barrier in the prototypical exchange of Cd^{2+} ions by Ag^{+} ions. A Wannier function-based tight binding model is employed to quantify microscopic mechanisms that influence this behavior. To support our model, we also tested our findings in a CE experiment: both CdSe and interstitially Ag-doped CdSe nanocrystals (containing 4% of Ag^{+} ions per nanocrystal on average) were exposed to Pb^{2+} ions at room temperature and it was observed that the exchange reaction proceeds further in doped nanocrystals. The findings suggest doping as a possible route to promote CE reactions that hardly undergo exchange otherwise, for example, those in III-V semiconductor nanocrystals.

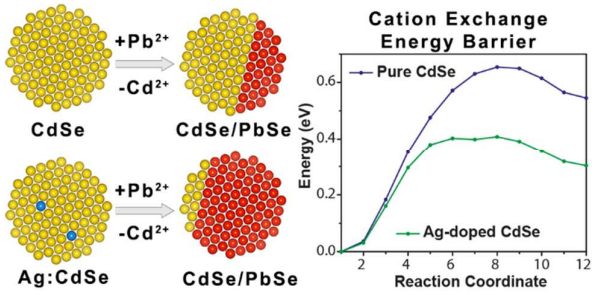

TEXT: Cation exchange (CE) reactions allow for selective replacement of cations of preformed ionic nanocrystals (NCs) with new desired guest cations, while retaining their size, shape and anion framework. This post-synthetic tool, coupled with the knowledge developed so far on colloidal synthesis, allows for the preparation of elaborate nanostructures,[1-6] with control over the morphology, composition and, in some cases, of the crystal structure. Hence, developing tools that would enable control of such reactions is of pressing interest. [7] On the other hand, the synthesis of specific nano-heterostructures or multinary NCs *via* CE reactions requires a deep understanding of the kinetics and/or the mechanisms of such transformations. Despite the vast amount of research since the last decade, a deep theoretical understanding of CE reactions is still lacking.[8-40] For example, no ways to control the exchange have been well established beyond increasing the temperature and the ion concentration in the solution. Indeed, it should be taken into account that performing CE reactions at elevated temperatures might lead to undesired side reactions, such as reduction of metal cations (in the presence of reductants such as alkylamines) or etching of the NCs[12]. Also, little is known about the possible influence of native ligands or impurities of the host colloidal NCs[1, 41] on the insertion and/or the extraction of the exchanging cations during a CE reaction.

This manuscript presents a theoretical study of the effects of interstitial doping on CE reactions, supported by our experimental findings. Starting from a prototypical exchange reaction between CdSe NCs and Ag^+ ions, we computed the contribution of each bond in the

system to the CE reaction barrier, using a Wannier function-based tight-binding Hamiltonian.[42-43] The results give quantitative insight into microscopic details of the exchange mechanism. Then we analyzed how the CE reaction barrier varies when interstitial Ni^{2+}, Ag^{+}, Hg^{2+} and Pb^{2+} impurities are present in the CdSe lattice, and found that local strain exerted by interstitial dopants on the surrounding ions loosened the Cd-Se bonds thus making them more prone to breaking during a CE reaction, so that the activation barrier of the CE transformation is considerably lowered. In order to verify these predictions, we synthesized both CdSe and Ag-doped CdSe NCs and tested them in CE reactions with Pb^{2+} ions. The choice of Ag-doped NCs as host NCs was motivated by the fact that Ag^{+} ions are known to interstitially dope CdSe NCs. When this occurs, the photoluminescence of the CdSe NCs increases.[44-45] The presence of silver impurities can thus be checked by both elemental analysis and through the increase of PL. Also, the exchange of Cd^{2+} ions with Pb^{2+} ions in CdSe is known to have a slow kinetics and requires a relatively high energy (i.e. high temperature) to get to completion.[46-48] The CE experiments, reported here show that the CdSe→PbSe transformation is significantly faster in NCs doped with Ag^{+} ions, lending support to our calculations.

In the present work, we have considered the prototypical Ag^{+} for Cd^{2+} CE reaction performed on CdSe NCs, and calculated the effect of interstitial impurities on the CE reaction barrier, within the so-called kick-out exchange mechanism.[49-50] The reaction scheme, depicted in **Figure 1**(a), is the following: a) in a CdSe NC a guest Ag^{+} cation, diffusing through interstitial positions, reaches one of the nearest sites around a Cd^{2+} cation; b) the Ag^{+} cation displaces the Cd^{2+} ion to the nearest interstitial site; c) the impurity occupies the closest interstitial site to the exchange event. The impurities considered in our computational model are M=Ni^{2+}, Ag^{+}, Hg^{2+} and Pb^{2+}, in the order of increasing ionic radius. Since larger impurities may not be stable in the interstitial positions, we also considered Li doping in Section S2 of the Supporting Information (SI). The

electronic structure varies from the center of the nanocrystal toward the surface. For the purpose of this work, we consider the impurity located deep inside the NC, and approximate the electronic structure of the CdSe NC by that of the bulk CdSe. Further, a low silver doping of 1.4 % is simulated by employing a 3x3x2 CdSe supercell containing a single Ag impurity. The Nudged Elastic Band (NEB) method[51] as implemented in Quantum Espresso (QE)[52] was used to sample reaction paths, while forces were computed from first principles,[53-54] in all calculations (see SI for more details).

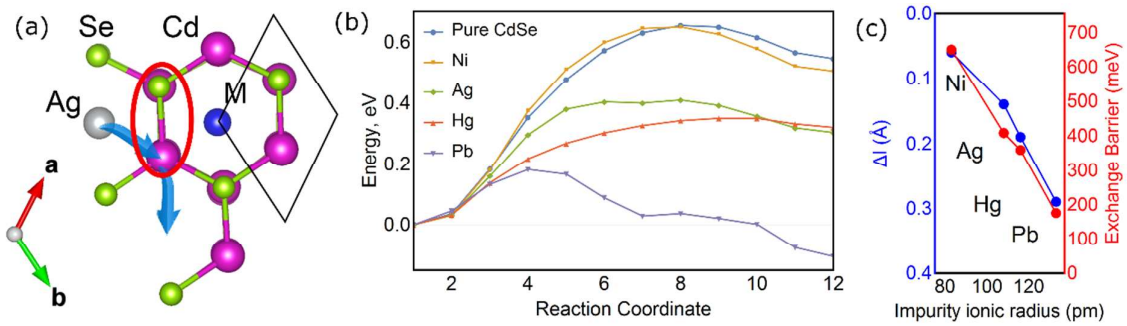

Figure 1. (a) Schematic representation of a cation exchange reaction in the host CdSe lattice in the presence of an impurity: a Cd ion adjacent to an interstitial impurity M is substituted by a silver ion. The impurity induces stretching of the neighboring bonds, one of which is highlighted by a red ellipse. The blue arrows indicate the migration of the ions during the CE "catalyzed" by the impurity. The unit cell of the undoped CdSe structure, containing 2 formula units, is shown by the black diamond. VESTA software[55] was used for plotting. (b) The activation barrier for the exchange of Cd^{2+} by Ag^{+} cations in CdSe NCs in the presence of impurities. (c) Elongation of the Cd-Se bond length, l (red ellipse in (a)), and the CE activation barrier as a function of the impurity radius.[56]

As shown in Figure 1 (b,c), a striking monotonous and nearly linear relation between the barrier height and the atomic radius of the impurity emerged from the calculations. This leads to

an exponential dependence of the CE rate on the ionic radius of the impurity. During a CE event, the Cd-Se bond, marked with a red ellipse in Figure 1 (a), breaks. The initial elongation of Cd-Se bond, Δl, which occurs due to the insertion of the interstitial impurity, depends on the ionic radius of the latter in a quasi-linear fashion, showing a very similar dependence to that of the activation barrier, as displayed in Figure 1 (c). A straightforward interpretation of the calculations is that the chemical bonds in the vicinity of the exchange event are weakened by the presence of the impurity. This suggests that, close to the impurity, the bond breaking events, necessary for the CE reaction, are less energetically costly and, thus, that a strain-aided CE activation could be possible.

Motivated by these findings we conducted a proof of concept experiment to test them. We synthesized both CdSe and Ag-doped CdSe NCs, in which silver dopants are known to occupy interstitial positions, and we used them as host NCs in CE reactions with Pb^{2+} ions. The inclusion of Ag dopants in CdSe NCs, obtained following the procedure reported by Sahu A. *et al.*[57] was confirmed by both inductively coupled plasma elemental analysis, through which we detected 4% of Ag^{+} ions inside the NCs, and the expected enhanced photoluminescence (PL) emission, peaked at 547nm, of the corresponding silver-doped NCs (see Figure 2 (a)). The size of the CdSe NCs, before and after the doping step, was extrapolated from the first absorption peak in the optical density spectra (see Figure 2 (a)) using a known size calibration curve,[58] which gave a diameter of 2 nm in both cases. The size is in line with what observed in transmission electron microscopy (TEM) images of the samples (see Figure S1 of the SI). As shown in Figure 2 (b,c) (black curves), the X-ray diffraction (XRD) patterns of both samples could be indexed with the wurtzite CdSe phase.[59] In order to study the Pb-for-Cd CE reaction in our NC systems we developed an *ad hoc* exchange reaction: the dispersion of NCs (either CdSe or silver-doped

CdSe) in toluene was mixed at room temperature with a methanolic solution containing an excess of lead acetate for either 20h or 2 days (see the Experimental Section in the SI for details). In published works, the CdSe → PbSe CE reaction is accomplished by using oleylamine, which preferentially binds Cd^{2+} ions, and it occurs only high temperatures (*i.e.* above ~100°C).[46-48] In our experimental settings, on the other hand, the transformation can occur at room temperature, driven by the lower solubility product constant of PbSe with respect to CdSe, which favors the formation of PbSe in the presence of a polar solvent (methanol in this case), preventing the so called "self-purification" of the NCs from dopant ions.[60] After 20h of CE with Pb^{2+} ions, the CdSe NCs were characterized by a PL emission having a maximum at 529nm (to be compared to 547nm of the starting CdSe NCs), and a composition of $CdPb_{0.1}Se$, as revealed by ICP elemental analysis (see Figure 2(b)). These results indicate that the size of the residual CdSe domains was reduced as a consequence of such exchange. However, only a small fraction of Cd^{2+} ions was exchanged with guest Pb^{2+} ions. On the other hand, Ag-doped CdSe NCs, after 20h of CE with Pb^{2+} ions, were characterized by a very weak PL emission, centered at 525nm, and their composition was $Cd_{0.8}Pb_{0.3}Se$ (with no presence of Ag), suggesting that in this sample the exchange proceeded to a higher extent.

After 48h of exchange with Pb^{2+} ions, both samples did not show any PL emission and the corresponding products were characterized by both XRD and elemental analyses. The XRD patterns of the CE products are shown in Figure 2 (c,d): in both cases, we clearly observed the presence of the original peaks ascribable to the wurtzite CdSe phase and the appearance of a new diffraction peak at 29.15° that can be univocally assigned to the rock-salt PbSe phase (clausthalite).[61]

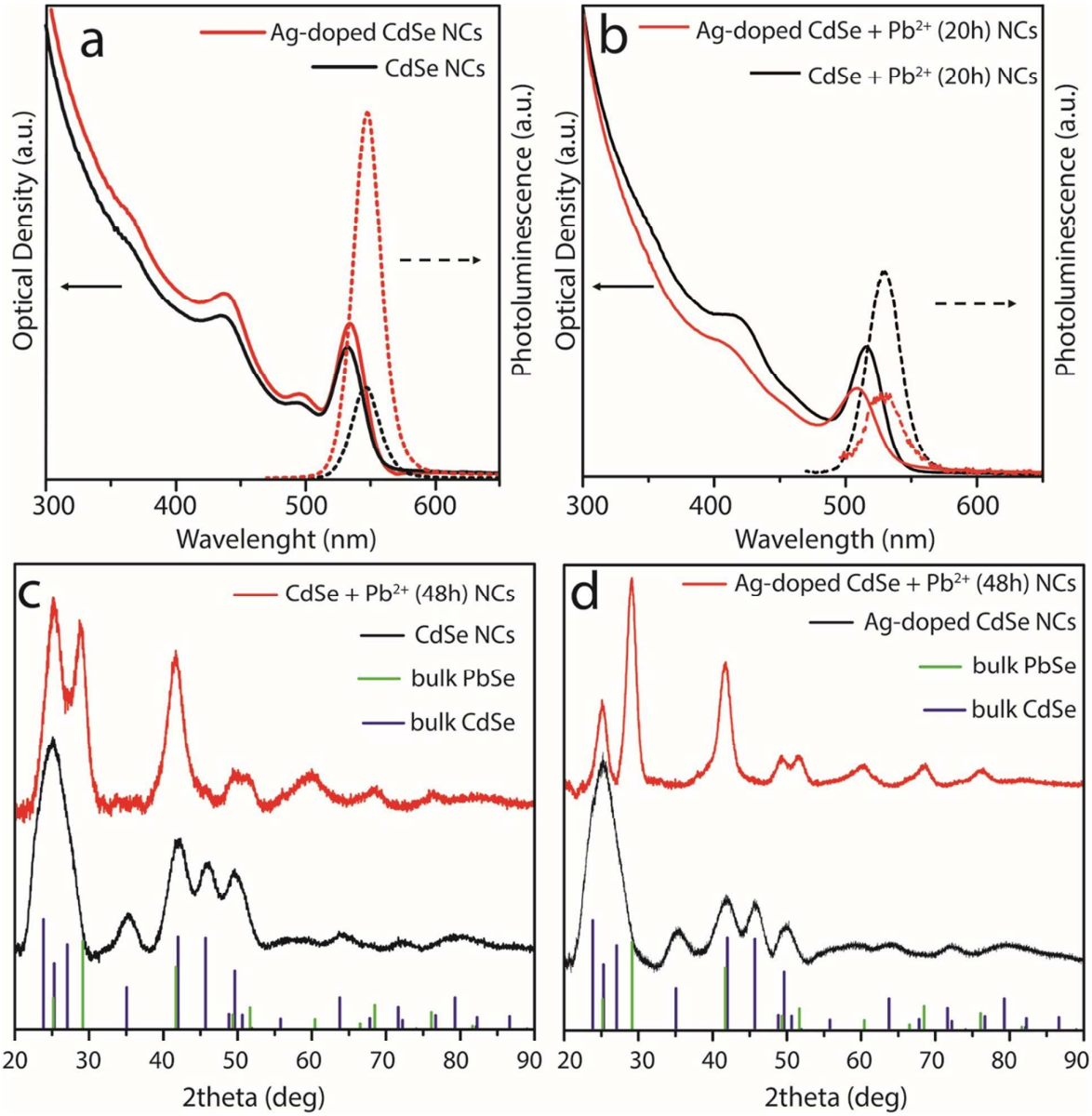

Figure 2. Absorption (solid line) and photoluminescence (dashed) spectra of CdSe NCs (in black) and Ag-doped CdSe NCs (in red) before (a) and after (b) 20h of CE with Pb^{2+} ions. (b,c) XRD patterns of the starting CdSe NCs and Ag-doped CdSe NCs (black lines) and of the corresponding products resulting from 48h of CE with Pb^{2+} ions (red lines). The bulk reflections of the wurtzite CdSe phase (ICSD 98-062-0414) and of the clausthalite PbSe (ICSD 98-98-007-6644) are also shown (blue and green bars, respectively).

Interestingly, the intensity of the peak at 29.15°, which is directly connected with the PbSe phase, was much more pronounced in the sample obtained starting from Ag-doped CdSe NCs, suggesting a higher degree of CdSe→PbSe conversion in this system, as seen in Figure 2. The ICP elemental analysis confirmed that the Pb^{2+} concentration in the product NCs was about 30% higher in the Ag-doped CdSe NCs: the stoichiometry changed from $Cd_{1.11}Se$ to $Cd_{0.49}Pb_{0.62}Se$ for the undoped system, and from $Cd_{1.15}Se$ to $Cd_{0.34}Pb_{0.83}Se$ for the Ag-doped one (in which no presence of Ag was detected after the CE reaction). Our TEM analysis also revealed that, upon CE, the NCs retained the initial size and shape, as shown in Figure S1 of the SI. These results indicate that the incorporation of silver in CdSe NCs accelerates the CE reaction.

The experimental and first principles data raise the intriguing question of what intrinsic microscopic mechanisms govern the CE reaction process. We have considered the same scheme as described above for the CE reaction modeling, but without an impurity and in a smaller unit cell (see SI for full details), and we developed a tight-binding model based on ab initio and NEB calculations to answer this question (see Figures S2 and S3 for further features of the model). The reaction barrier obtained is a combination of different energy contributions. In the framework of DFT, we can decompose the total energy as a sum of Coulomb energies (including Ewald contribution, Hartree contribution and exchange-correlation energy) and the kinetic or band energy, corresponding to the single particle Kohn-Sham energies.[52]

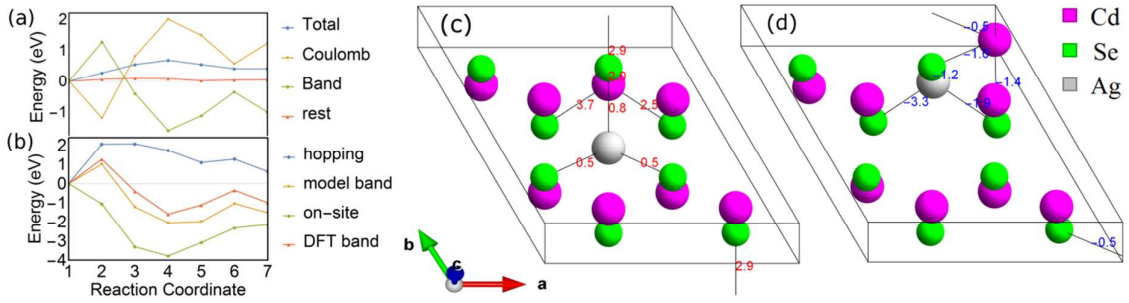

Figure 3. (a) Decomposition of the CE energy barrier, calculated within DFT, on electronic kinetic energy, Coulomb energy, including the Ewald, exchange and Hartree contributions, and the rest, including the one-center PAW and the smearing contributions; (b) Decomposition of the electronic kinetic energy (orange) of the tight binding model into on-site (green) and hopping energy (blue). The band energy calculated within DFT (red) closely approximates that obtained from the tight binding model; the most significant positive (c) and negative (d) bonding energy changes from the initial configuration (interstitial Ag) to the configuration at the top of the CE barrier. Negative numbers (in blue) indicate energy gain and bond formation, while positive (energy loss) indicate bond weakening or breaking.

Coulomb forces have been identified in the seminal work of Ott *et al.*[62] as an important factor in the exchange processes accounting in part for the decrease in the reaction barrier after the first exchange event has taken place. Figure 3 (a,b) shows the cation exchange energy barrier at fixed lattice parameters, alongside the decomposition of this barrier into kinetic and Coulomb-like contributions from our simulations. We can see that the two kinetic and Coulomb contributions have nearly-opposite values up to five times larger than the barrier itself.

To isolate contributions to energy change from different bonds and gain an insight into electronic structure changes during CE, we have performed Wannier interpolation of the band structure by a tight binding Hamiltonian, employing the Wannier90 code[63-64] (see more details in the SI). To ensure that the Wannier functions change as little as possible along the reaction path, we have used the same projection functions for Wannier interpolation for all images and turned off the maximal localization procedure.

The Hamiltonian for a paramagnetic state may be written as

$$H^{TB} = \sum_{i,j,R,R',\sigma} t_{ij}^{RR'} \psi_{i,R,\sigma}^{+} \psi_{j,R',\sigma}$$

where $\psi_{i,R,\sigma}^{+}$ creates an electron with spin σ in the orbital *i* at the unit cell ***R***, while the term with $t_{ij}^{RR'}$ quantifies the hopping integral between Wannier orbitals *i* and *i'* residing in the unit cells ***R*** and ***R'*** respectively. In the following we refer to the terms with ***R***=***R'*** and *i*=*j* as on-site terms, and to others as hopping terms.

During the reaction, many orbitals along the path of the exchanging cations are affected. It is therefore natural that many hopping amplitudes change. This reinforces the picture in which a CE reaction is viewed as a sequence of bond breaking-bond creation events. Bonding can be quantified using the kinetic energy gain due to delocalization of an electron between orbitals *i* and *j*, residing in unit cells ***R*** and ***R'***. This is given by

$$\varepsilon_{ij}^{RR'} = \frac{2}{N} \sum_{\boldsymbol{k},\sigma} \sum_{n} Re[t_{ij}^{\boldsymbol{RR'}} c_{i,\boldsymbol{R},\sigma}^{n,\boldsymbol{k}*} c_{j,\boldsymbol{R'},\sigma}^{n,\boldsymbol{k}} e^{i\boldsymbol{k}(\boldsymbol{R'}-\boldsymbol{R})}] f_{F-D}^{n,\boldsymbol{k}}$$

where $c_{i,\boldsymbol{R}}^{n,\boldsymbol{k}}$ is the projection of the nth band Bloch function at ***k*** on the orbital *i* located at site ***R***, $f_{F-D}^{n,\boldsymbol{k}}$ is the value of the Fermi-Dirac distribution function for the electronic band n at point ***k*** and N is the number of ***k*** points in the grid. A derivation of these expressions can be found in the SI. This approach gives the bond-resolved electronic energy and allows to quantify the changes in the bonding along the CE reaction path. The calculations were performed using the *Bondener* package[65] (see SI for details).

The decomposition of the kinetic energy into Coulomb-like and kinetic energies gives insight into the reaction mechanism. In particular, we determine the decomposition of the energy barrier into hopping and onsite contributions, as shown in Figure 3 (a,b). The evolution of the hopping energy suggests extensive Cd-Se bond breaking at the first stage and then a progressive readjustment until a low hopping energy arrangement is reached, with the Cd^{2+} cation relaxed in

the interstitial and the Ag^+ cation forming bonds with neighboring Se^{2-} ions. This pure-hopping-energy contribution to the energy barrier is similar in importance to the Coulomb-like contribution, with a peak of about 2 eV. The tight-binding model with truncated long-range terms does reproduce the DFT band energy.

The formalism allows to decompose the kinetic energy and the CE barrier into per-bond contributions, highlighting the most important changes in bonding through the reaction. Classifying kinetic energy terms with the largest change from image 1 (initial state) to image 4 (top of the barrier), we verify that it is the breaking-bond, indicated in a red ellipse in Figure 1, that experiences the largest energy gain through the process. In Figure 3 (c,d) are shown the largest bond energy changes (energy gain and loss, respectively) on the corresponding atoms in the structure. In addition, we calculate the contributions of all relevant orbitals, which are depicted in the piechart shown in Figure S4 of the SI. The largest individual contributions are coming from the on-site terms corresponding to the s orbitals of the two cations migrating during the exchange, Ag^+ and Cd^{2+}. This can be attributed to the strong environmental change the cations experience. The largest single hopping energy contribution corresponds to the Cd_p-Se_p bond breaking, shown in Figure S5 in the SI. The largest hopping energy loss falls on the Ag_p-Se_p bonding energy, lost in the final configuration of the reaction. Interestingly, all bond energy losses above the 0.35 eV threshold involve the Ag^+ cation, which is approaching the substitutional position and effectively forming bonds. On the other hand, the five largest bonding energy gains involve hopping between the migrating Cd^{2+} ion and the surrounding Se^{2-} ions, indicating bond breaking. Therefore, the results of the quantitative analysis resemble the intuition quite remarkably.

Finally, the fact that a large number of smaller hopping terms is needed for an accurate description of the exchange barrier suggests a strong connection of the energetic picture to the

proposed strain-mediated mechanism: the CE barrier energy, though strongly contributed by local bond breaking and creation processes, is "paid" also in terms of interactions of longer range, indicating a collective response of the crystal, corresponding to lattice strain. In Figure S6 in the SI we calculate explicitly the effect of lattice strain in two different settings, to illustrate this point.

In summary, we present theoretical and experimental evidence that suggests that interstitial doping in CdSe nanocrystals accelerates their CE reactions with guest cations such as Pb^{2+}. The theoretical method presented breaks the ground for the systematic study of cation exchange reaction barriers from a quantitative point of view, and the results offer a new insight in the microscopic mechanism of the process. We have demonstrated a key role of the interstitial impurities in inducing cation exchange in nanocrystals. Despite other important factors intrinsic to the complexity of CE in colloidal nanocrystals, our experimental data and theoretical analysis suggest that CE induced by interstitial impurities can be used to control the composition of a new class of NCs. We expect these results will motivate further studies of the doping-assisted CE.

ASSOCIATED CONTENT

Supporting information

Contains: experimental details about synthesis of the NC, cation exchange reactions, XRD measurements, elemental analysis, optical absorption measurements and photoluminescence measurements. Additional technical details about DFT calculations; derivation of the bond energy per pair of orbitals, details about the tight binding model used and the decomposition of the energies calculated. Information on the effect of strain on the reaction barrier under other settings.

AUTHOR INFORMATION

Corresponding Authors

Luca De Trizio (Luca.DeTrizio@iit.it), Liberato Manna (Liberato.Manna@iit.it), Sergey Artyukhin (Sergey.Artyukhin@iit.it)

Present Addresses

†Glass to Power Srl, Via Roberto Cozzi, 55, Milan 20125, Italy

ACKNOWLEDGMENT

This work was supported by the FP7 ERC Consolidator Grant TRANS NANO (contract n. 614897), by framework programme for research and Innovation Horizon 2020 (2014-2020) under the Marie Skłodowska-Curie Grant Agreement COMPASS No. 691185, and the computational resources from CINECA supercomputing center are acknowledged.

REFERENCES

1. Erwin, S. C.; Zu, L.; Haftel, M. I.; Efros, A. L.; Kennedy, T. A.; Norris, D. J. Doping semiconductor nanocrystals. *Nature* **2005,** *436*, 91-94.
2. Jia, G.; Sitt, A.; Hitin, G. B.; Hadar, I.; Bekenstein, Y.; Amit, Y.; Popov, I.; Banin, U. Couples of colloidal semiconductor nanorods formed by self-limited assembly. *Nat. Mater.* **2014,** *13*, 301-307.
3. Kovalenko, M. V.; Manna, L.; Cabot, A.; Hens, Z.; Talapin, D. V.; Kagan, C. R.; Klimov, V. I.; Rogach, A. L.; Reiss, P.; Milliron, D. J.; et al. Prospects of nanoscience with nanocrystals. *ACS Nano* **2015,** *9*, 1012-1057.
4. Rivest, J. B.; Jain, P. K. Cation exchange on the nanoscale: an emerging technique for new material synthesis, device fabrication, and chemical sensing. *Chem. Soc. Rev.* **2013,** *42*, 89-96.
5. Talapin, D. V.; Lee, J. S.; Kovalenko, M. V.; Shevchenko, E. V. Prospects of colloidal nanocrystals for electronic and optoelectronic applications. *Chem. Rev.* **2010,** *110*, 389-458.
6. Luther, J. M.; Zheng, H.; Sadtler, B.; Alivisatos, A. P. Synthesis of PbS Nanorods and Other Ionic Nanocrystals of Complex Morphology by Sequential Cation Exchange Reactions. *J. Am. Chem. Soc.* **2009,** *131*, 16851–16857.

7. Zhang, Q.; Yin, K.; Dong, H.; Zhou, Y.; Tan, X.; Yu, K.; Hu, X.; Xu, T.; Zhu, C.; Xia, W.; et al. Electrically driven cation exchange for in situ fabrication of individual nanostructures. *Nat. Commun.* **2017,** *8*, 14889.
8. Beberwyck, B. J.; Surendranath, Y.; Alivisatos, A. P. Cation Exchange: A Versatile Tool for Nanomaterials Synthesis. *J. Phys. Chem. C* **2013,** *117*, 19759-19770.
9. Chakraborty, P.; Jin, Y.; Barrows, C. J.; Dunham, S. T.; Gamelin, D. R. Kinetics of Isovalent (Cd2+) and Aliovalent (In3+) Cation Exchange in Cd1-xMnxSe Nanocrystals. *J. Am. Chem. Soc.* **2016,** *138*, 12885-12893.
10. Chan, E. M.; Marcus, M. A.; Fakra, S.; ElNaggar, M.; Mathies, R. A.; Alivisatos, A. P. Millisecond kinetics of nanocrystal cation exchange using microfluidic X-ray absorption spectroscopy. *J. Phys. Chem. A* **2007,** *111*, 12210-12215.
11. Choi, J. Y.; Lee, S. J.; Seo, W. S.; Song, H. Air-stable CuInSe2 nanoparticles formed through partial cation exchange in methanol at room temperature. *Crystengcomm* **2016,** *18*, 6069-6075.
12. De Trizio, L.; Manna, L. Forging Colloidal Nanostructures via Cation Exchange Reactions. *Chem. Rev.* **2016,** *116*, 10852-10887.
13. Doh, H.; Hwang, S.; Kim, S. Size-Tunable Synthesis of Nearly Monodisperse Ag2S Nanoparticles and Size-Dependent Fate of the Crystal Structures upon Cation Exchange to AgInS2 Nanoparticles. *Chem. Mater.* **2016,** *28*, 8123-8127.
14. Dzhagan, V.; Kempken, B.; Valakh, M.; Parisi, J.; Kolny-Olesiak, J.; Zahn, D. R. T. Probing the structure of CuInS2-ZnS core-shell and similar nanocrystals by Raman spectroscopy. *Appl. Surf. Sci.* **2017,** *395*, 24-28.
15. Enright, M. J.; Sarsito, H.; Cossairt, B. M. Quantifying Cation Exchange of Cd2+ in ZnTe: A Challenge for Accessing Type II Heterostructures. *Chem. Mater.* **2017,** *29*, 666-672.
16. Fan, Z. C.; Lin, L. C.; Buijs, W.; Vlugt, T. J. H.; van Huis, M. A. Atomistic understanding of cation exchange in PbS nanocrystals using simulations with pseudoligands. *Nat. Commun.* **2016,** *7*, 11503.
17. Fenton, J. L.; Schaak, R. E. Structure-Selective Cation Exchange in the Synthesis of Zincblende MnS and CoS Nanocrystals. *Angew. Chem., Int. Ed.* **2017,** *56*, 6464-6467.
18. Gabka, G.; Bujak, P.; Kotwica, K.; Ostrowski, A.; Lisowski, W.; Sobczak, J. W.; Pron, A. Luminophores of tunable colors from ternary Ag-In-S and quaternary Ag-In-Zn-S nanocrystals covering the visible to near-infrared spectral range. *Phys. Chem. Chem. Phys.* **2017,** *19*, 1217-1228.
19. Gupta, S.; Kershaw, S. V.; Rogach, A. L. 25th Anniversary Article: Ion Exchange in Colloidal Nanocrystals. *Adv. Mater.* **2013,** *25*, 6923-6943.
20. Han, S. Y.; Qin, X.; An, Z. F.; Zhu, Y. H.; Liang, L. L.; Han, Y.; Huang, W.; Liu, X. G. Multicolour synthesis in lanthanide-doped nanocrystals through cation exchange in water. *Nat. Commun.* **2016,** *7*, 13059.
21. Jang, Y. J.; Yanover, D.; Capek, R. K.; Shapiro, A.; Grumbach, N.; Kauffmann, Y.; Sashchiuk, A.; Lifshitz, E. Cation Exchange Combined with Kirkendall Effect in the Preparation of SnTe/CdTe and CdTe/SnTe Core/Shell Nanocrystals. *J. Phys. Chem. Lett.* **2016,** *7*, 2602-2609.
22. Kershaw, S. V.; Abdelazim, N. M.; Zhao, Y. H.; Susha, A. S.; Zhovtiuk, O.; Teoh, W. Y.; Rogach, A. L. Investigation of the Exchange Kinetics and Surface Recovery of CdxHg1-xTe Quantum Dots during Cation Exchange Using a Microfluidic Flow Reactor. *Chem. Mater.* **2017,** *29*, 2756-2768.
23. Lee, S.; Baek, S.; Park, J. P.; Park, J. H.; Hwang, D. Y.; Kwak, S. K.; Kim, S. W. Transformation from Cu2-xS Nanodisks to Cu2-xS@CuInS2 Heteronanodisks via Cation Exchange. *Chem. Mater.* **2016,** *28*, 3337-3344.
24. Luo, Z. S.; Irtem, E.; Ibanez, M.; Nafria, R.; Marti-Sanchez, S.; Genc, A.; de la Mata, M.; Liu, Y.; Cadavid, D.; Llorca, J.; et al. Mn3O4@CoMn2O4 CoxOy Nanoparticles: Partial Cation Exchange Synthesis and Electrocatalytic Properties toward the Oxygen Reduction and Evolution Reactions. *ACS Appl. Mater. Interfaces* **2016,** *8*, 17435-17444.

25. Meir, N.; Martin-Garcia, B.; Moreels, I.; Oron, D. Revisiting the Anion Framework Conservation in Cation Exchange Processes. *Chem. Mater.* **2016,** *28*, 7872-7877.
26. Ramasamy, P.; Kim, M.; Ra, H. S.; Kim, J.; Lee, J. S. Bandgap tunable colloidal Cu-based ternary and quaternary chalcogenide nanosheets via partial cation exchange. *Nanoscale* **2016,** *8*, 7906-7913.
27. Roudebush, J. H.; Ross, K. A.; Cava, R. J. Iridium containing honeycomb Delafossites by topotactic cation exchange. *Dalton Trans.* **2016,** *45*, 8783-8789.
28. Saha, A.; Makkar, M.; Shetty, A.; Gahlot, K.; Pavan, A. R.; Viswanatha, R. Diffusion doping in quantum dots: bond strength and diffusivity. *Nanoscale* **2017,** *9*, 2806-2813.
29. Son, D. H.; Hughes, S. M.; Yin, Y.; Paul Alivisatos, A. Cation exchange reactions in ionic nanocrystals. *Science* **2004,** *306*, 1009-1012.
30. Song, J. L. Q.; Ma, C.; Zhang, W. Z.; Li, X. D.; Zhang, W. T.; Wu, R. B.; Cheng, X. C.; Ali, A.; Yang, M. Y.; Zhu, L. X.; et al. Bandgap and Structure Engineering via Cation Exchange: From Binary Ag2S to Ternary AgInS2, Quaternary AgZnInS alloy and AgZnInS/ZnS Core/Shell Fluorescent Nanocrystals for Bioimaging. *ACS Appl. Mater. Interfaces* **2016,** *8*, 24826-24836.
31. Sun, Z. J.; Liu, X.; Yue, Q. D.; Jia, H. X.; Du, P. W. Cadmium Sulfide Nanorods Decorated with Copper Sulfide via One-Step Cation Exchange Approach for Enhanced Photocatalytic Hydrogen Evolution under Visible Light. *Chemcatchem* **2016,** *8*, 157-162.
32. Tan, C. S.; Lu, Y. J.; Chen, C. C.; Liu, P. H.; Gwo, S.; Guo, G. Y.; Chen, L. J. Magnetic MoS2 Interface Monolayer on a CdS Nanowire by Cation Exchange. *J. Phys. Chem. C* **2016,** *120*, 23055-23060.
33. Tang, Y. F.; Chen, S. J.; Mu, S. C.; Chen, T.; Qiao, Y. Q.; Yu, S. X.; Gao, F. N. Synthesis of Capsule-like Porous Hollow Nanonickel Cobalt Sulfides via Cation Exchange Based on the Kirkendall Effect for High-Performance Supercapacitors. *ACS Appl. Mater. Interfaces* **2016,** *8*, 9721-9732.
34. Teitelboim, A.; Oron, D. Broadband Near-Infrared to Visible Upconversion in Quantum Dot-Quantum Well Heterostructures. *ACS Nano* **2016,** *10*, 446-452.
35. Wang, Y. X.; Morozov, Y. V.; Zhukovskyi, M.; Chatterjee, R.; Draguta, S.; Tongying, P.; Bryant, B.; Rouvimov, S.; Kuno, M. Transforming Layered to Nonlayered Two-Dimensional Materials: Cation Exchange of SnS2 to Cu2SnS3. *ACS Energy Lett.* **2016,** *1*, 175-181.
36. White, S. L.; Smith, J. G.; Behl, M.; Jain, P. K. Co-operativity in a nanocrystalline solid-state transition. *Nat. Commun.* **2013,** *4*, 2933.
37. Wu, W. Y.; Chakrabortty, S.; Guchhait, A.; Wong, G. Y. Z.; Dalapati, G. K.; Lin, M.; Chan, Y. T. Solution-Processed 2D PbS Nanoplates with Residual Cu2S Exhibiting Low Resistivity and High Infrared Responsivity. *Chem. Mater.* **2016,** *28*, 9132-9138.
38. Xu, Y. Z.; Yuan, C. Z.; Chen, X. P. Co-Doped NiSe nanowires on nickel foam via a cation exchange approach as efficient electrocatalyst for enhanced oxygen evolution reaction. *RSC Adv.* **2016,** *6*, 106832-106836.
39. Zhang, C. W.; Xia, Y.; Zhang, Z. M.; Huang, Z.; Lian, L. Y.; Miao, X. S.; Zhang, D. L.; Beard, M. C.; Zhang, J. B. Combination of Cation Exchange and Quantized Ostwald Ripening for Controlling Size Distribution of Lead Chalcogenide Quantum Dots. *Chem. Mater.* **2017,** *29*, 3615-3622.
40. Zheng, Z. Y.; Sun, Y. Y.; Xie, W. Y.; Zhao, J. J.; Zhang, S. B. Solvent-Based Atomistic Theory for Doping Colloidal-Synthesized Quantum Dots via Cation Exchange. *J. Phys. Chem. C* **2016,** *120*, 27085-27090.
41. Chen, H. Y.; Son, D. H. Energy and Charge Transfer Dynamics in Doped Semiconductor Nanocrystals. *Isr. J. Chem.* **2012,** *52*, 1016-1026.
42. Bloch, F. über die Quantenmechanik der Elektronen in Kristallgittern. *Z. Phys.* **1928,** *52*, 555-600.
43. Wannier, G. H. The Structure of Electronic Excitation Levels in Insulating Crystals. *Phys. Rev.* **1937,** *52*, 191.
44. Gopal, M. B. Ag and Cu doped colloidal CdSe nanocrystals: partial cation exchange and luminescence. *Mater. Res. Express* **2015,** *2*, 085004.

45. Kompch, A.; Sahu, A.; Notthoff, C.; Ott, F.; Norris, D. J.; Winterer, M. Localization of Ag Dopant Atoms in CdSe Nanocrystals by Reverse Monte Carlo Analysis of EXAFS Spectra. *J. Phys. Chem. C* **2015,** *119*, 18762-18772.
46. Lee, D.; Kim, W. D.; Lee, S.; Bae, W. K.; Lee, S.; Lee, D. C. Direct Cd-to-Pb Exchange of CdSe Nanorods into PbSe/CdSe Axial Heterojunction Nanorods. *Chem. Mater.* **2015,** *27*, 5295-5304.
47. Zhang, J. B.; Chernomordik, B. D.; Crisp, R. W.; Kroupa, D. M.; Luther, J. M.; Miller, E. M.; Gao, J. B.; Beard, M. C. Preparation of Cd/Pb Chalcogenide Heterostructured Janus Particles via Controllable Cation Exchange. *ACS Nano* **2015,** *9*, 7151-7163.
48. Zhang, J. B.; Gao, J. B.; Church, C. P.; Miller, E. M.; Luther, J. M.; Klimov, V. I.; Beard, M. C. PbSe Quantum Dot Solar Cells with More than 6% Efficiency Fabricated in Ambient Atmosphere. *Nano Lett.* **2014,** *14*, 6010-6015.
49. Bothe, C.; Kornowski, A.; Tornatzky, H.; Schmidtke, C.; Lange, H.; Maultzsch, J.; Weller, H. Solid-State Chemistry on the Nanoscale: Ion Transport through Interstitial Sites or Vacancies? *Angew. Chem., Int. Ed.* **2015,** *54*, 14183-14186.
50. Gösele, U.; Frank, W.; Seeger, A. Mechanism and kinetics of the diffusion of gold in silicon. *Appl. Phys. A: Solids Surf.* **1980,** *23*, 361–368.
51. Mills, G.; Jonsson, H.; Schenter, G. K. Reversible Work Transition-State Theory - Application to Dissociative Adsorption of Hydrogen. *Surf. Sci.* **1995,** *324*, 305-337.
52. Giannozzi, P.; Baroni, S.; Bonini, N.; Calandra, M.; Car, R.; Cavazzoni, C.; Ceresoli, D.; Chiarotti, G. L.; Cococcioni, M.; Dabo, I.; et al. QUANTUM ESPRESSO: a modular and open-source software project for quantum simulations of materials. *J. Phys.: Condens. Matter.* **2009,** *21*, 395502.
53. Hohenberg, P.; Kohn, W. Inhomogeneous Electron Gas. *Phys. Rev.* **1964,** *136*, B864.
54. Kohn, W.; Sham, L. J. Self-Consistent Equations Including Exchange and Correlation Effects. *Phys. Rev.* **1965,** *140*, A1133.
55. Momma, K.; Izumi, F. VESTA 3 for three-dimensional visualization of crystal, volumetric and morphology data. *J. Appl. Crystallogr.* **2011,** *44*, 1272-1276.
56. Shannon, R. D. Revised effective ionic radii and systematic studies of interatomic distances in halides and chalcogenides. *Acta Crystallogr.* **1976,** *A32*, 751-767.
57. Sahu, A.; Kang, M. S.; Kompch, A.; Notthoff, C.; Wills, A. W.; Deng, D.; Winterer, M.; Frisbie, C. D.; Norris, D. J. Electronic impurity doping in CdSe nanocrystals. *Nano Lett.* **2012,** *12*, 2587-2594.
58. Jasieniak, J.; Smith, L.; van Embden, J.; Mulvaney, P.; Califano, M. Re-examination of the Size-Dependent Absorption Properties of CdSe Quantum Dots. *J. Phys. Chem. C* **2009,** *113*, 19468-19474.
59. Climent Montoliu, F.; Rodriguez Lopez, J. L. Synthesis and x-ray diffraction structural study of zinc selenide and cadmium selenide. *An. Quim., Ser. B* **1984,** *80*, 172-175.
60. Dalpian, G. M.; Chelikowsky, J. R. Self-purification in semiconductor nanocrystals. *Phys. Rev. Lett.* **2006,** *96*, 226802.
61. Earley, J. W. Description and Synthesis of the Selenide Minerals. *Am. Mineral.* **1950,** *35*, 337-364.
62. Ott, F. D.; Spiegel, L. L.; Norris, D. J.; Erwin, S. C. Microscopic Theory of Cation Exchange in CdSe Nanocrystals. *Phys. Rev. Lett.* **2014,** *113,* 156803.
63. Marzari, N.; Vanderbilt, D. Maximally localized generalized Wannier functions for composite energy bands. *Phys. Rev. B* **1997,** *56*, 12847-12865.
64. Mostofi, A. A.; Yates, J. R.; Pizzi, G.; Lee, Y. S.; Souza, I.; Vanderbilt, D.; Marzari, N. An updated version of wannier90: A tool for obtaining maximally-localised Wannier functions. *Comput. Phys. Commun.* **2014,** *185*, 2309-2310.
65. Petralanda, U.; Artyukhin, S. *Bondener -- a tool for Wannier function-based bonding analysis [Online]*, https://github.com/UrkoPH/bondener, 2017.